Inertial Embedded Fronts

WILLIAM K. DEWAR

Department of Oceanography, The Florida State University, Tallahassee, Florida

JOHN C. MARSHALL

Department of Earth, Atmosphere, and Planetary Sciences, Massachusetts Institute of Technology, Cambridge, Massachusetts

(Manuscript received 4 December 1991, in final form 1 February 1993)

ABSTRACT

Many recent observations have described fronts in the interior of the ocean at locations far away from any lateral boundaries. Some of these fronts are observed to be associated with considerable mass transports, which suggests that they participate importantly in setting the water mass structure of the ocean interior, and represent considerable local departures from linear Sverdrup dynamics. In this paper, a simple analytic theory of interior fronts is developed. The main features of this theory are that the fronts are highly inertial and anisotropic, and reside on the edge of a somewhat larger scale interior inertial recirculation. The recirculation is taken to be modonlike; the dynamic height difference across the edge of the recirculation supports an interior jet, which is clockwise around the edge of the recirculation and carries water from the subpolar into the subtropical gyre. Unlike in previous theories of interior fronts, all of the transports, both in the large-scale and the fronts, are "anomalous" and in excess of any wind-driven transport. The fronts themselves represent interior, deformation-scale boundary layers, which are necessary to smoothly join the baroclinic parts of the inertial recirculation and the sluggish Sverdrup zones. The authors speculate on the role of these dynamics in the LDE jet.

1. Introduction

A remarkable observation of a surface-intensified open-ocean jet was obtained during the Local Dynamics Experiment (McWilliams et al. 1983). This jet had near-surface (200 db) flows to the southwest in excess of 30 cm s^{-1}, was surface intensified (but may have been dynamically present to depths of 3000 db), and exhibited a strong baroclinic signal (e.g., the 15°C isotherm, centered at ~550 m, shallowed by 200 m moving east across the jet). The scales of the jet were decidedly anisotropic, with a cross-front scale O(50–100 km) and an alongfront scale that ultimately was not resolved by the experiment, but was determined to be at least 400 km.

This jet was observed just south and west of Bermuda, in a region commonly thought of as on the edge of the North Atlantic so-called inertial recirculation. Although the greatest bulk of the data describing the jet was hydrographic (obtained during the intensive hydrographic period), the jet axis wandered over individual LDE current meter moorings during the experiment. Some of the current meter data showed the jet vertical profile to be to the southwest, that is, in a sense opposite to that of the Gulf Stream, throughout the water column. These observations suggested that the dynamic method relative to 3000 db could be used to estimate the jet transport, an exercise yielding a remarkable transport estimate of 40 Sv (Sv $\equiv 10^6$ m^3 s^{-1}). Note this transport is comparable in magnitude to the northward Gulf Stream transport farther west at the same latitude and, questions of persistence aside, argues strongly that the LDE jet constituted a major feature of the large-scale North Atlantic circulation.

The theory of such interior fronts is not well developed and important types of possible jet structure have not yet been dynamically examined. The purpose of this paper is to present a simple analytical theory of interior fronts, with the objective of exploring dynamics that might play some role in the LDE jet.

Background

The theoretical study of baroclinic midocean fronts is relatively limited, with principal references being Cushman-Roisin (1984), Luyten and Stommel (1986), and Dewar (1991a,b). A common feature of these studies is that they are governed fundamentally by Sverdrup dynamics, so that net barotropic transport is set by the wind. The thermocline in baroclinic general circulation ocean models subject to such a constraint is determined by characteristics emanating from either the eastern or western boundary. Distinct regions of

Corresponding author address: Dr. William K. Dewar, Department of Oceanography B-169, The Florida State University, Tallahassee, FL 32306-3048.

ocean basins are thus controlled by one of these two boundaries, a result first made explicit in the homogenization theories of Rhines and Young (1982a,b). Cushman-Roisin (1984) demonstrated that these distinct sets of characteristics could overlap in a buoyantly and mechanically driven subtropical gyre, and identified the region of overlap with the subtropical countercurrent of the North Pacific. Dewar (1991a) demonstrated the existence of such fronts in a purely adiabatic subtropical–subpolar gyre model and illustrated the coupling between the dynamics of the front and the thermocline structure of the gyre. The application of these ideas to the ventilated thermocline was discussed in Dewar (1991b).

These studies illustrate many interesting aspects of midocean fronts; however, some data, like those associated with the LDE jet, suggest midocean fronts can have properties that the previous studies lack. Most importantly, the fronts they describe obey the Sverdrup constraint and hence are responsible for a net barotropic transport that scales as the jet width and is small. The LDE jet, however, appeared to transport a volume of water southward that could not possibly be accounted for by Sverdrup dynamics (here we shall refer to such transports as "anomalous"). This argues that a potentially important aspect of LDE jet dynamics is absent from the above models. Second, the fronts in the above models were entirely embedded within a Sverdrup flow. It is commonly accepted, however, that the circulation of the northwest corner of the subtropical North Atlantic gyre is dynamically distinct from that of the North Atlantic interior; the latter seems broadly in accord with linear Sverdrup dynamics while the former appears much more inertial in character. This is connected to the well known increase in Gulf Stream transport (from ~40 to ~150 Sv) downstream from Cape Hatteras, among other things. With respect to the LDE jet, its observed location is suggestively close to the eastern edge of this so-called inertial recirculation, suggesting an interaction of the front with the recirculation. It is this interaction that is missing from previous theories.

In this paper, a simple analytical model of fronts in the presence of inertial recirculation is discussed. Our objectives are to present a first-order theory of the structure of interior fronts in these circumstances and to describe their associated dynamics. In contrast to previous models, wind forcing is excluded at the outset. Hence, any and all meridional transport in this model is by definition anomalous with respect to the (vanishing) Sverdrup transport. Interior circulations are driven by inflow conditions at an inlet port on the western central boundary, which is meant to represent the influx of mass from the Gulf Stream. The circumstances yielding interior baroclinic fronts appear naturally and measures of their transport are obtained.

We find that fronts arise as a result of inconsistency between the boundary conditions located at the eastern and western basin edges. This result mirrors the earlier analyses of fronts in Sverdrup flows. However, the inertial gyres obtained here are relatively limited in their north–south extent and this tends to weaken the westward, beta-driven propagation tendencies of the fronts. This, combined with the strength of the inertial recirculation, traps the fronts at the edge of the recirculation. In effect, the fronts play the role of an internal boundary layer that smoothly joins the inertial recirculation and the less energetic far field. Although narrow, the transport of the fronts can be sizeable.

This highly idealized model has mass source zones in the subpolar gyre. In view of this, it is interesting that anomalous water masses of apparently subpolar origin were found in the LDE jet. Thus, we speculate that the present model, in spite of its highly idealized nature and obvious shortcomings with respect to the LDE jet, may illustrate some of the dynamics that participated in that event.

The physical system and supporting scale analysis is developed in the next section and solutions of the combined barotropic/baroclinic system are discussed in section 3. A discussion of the model and the LDE jet concludes the paper.

2. Model development

The ocean will be modeled as a rotating two-layer, flat-bottomed Boussinesq fluid of total depth H (see Fig. 1). The Coriolis parameter will be denoted $f = f_0 + \beta y$ (using conventional notation) and the reduced gravity parameter will be denoted g'. Upper-layer velocities will be denoted as $\mathbf{u}$ and lower-layer velocities by $\mathbf{v}$; upper-layer dynamic pressure will be denoted by p_1, upper-layer thickness by h, and lower-layer pressure by p; x and y are east and north coordinates, respectively, and steady solutions will be sought. Under these conditions, the dimensional equations of motion are

$$\mathbf{u}\cdot\nabla\mathbf{u} + f\mathbf{k}\times\mathbf{u} = -\nabla p_1 = -\nabla(p+h) \quad (1a)$$

$$\nabla\cdot(\mathbf{u}h) = 0 \quad (1b)$$

$$\mathbf{v}\cdot\nabla\mathbf{v} + f\mathbf{k}\times\mathbf{v} = -\nabla(p) \quad (1c)$$

$$\nabla\cdot[\mathbf{v}(H-h)] = 0. \quad (1d)$$

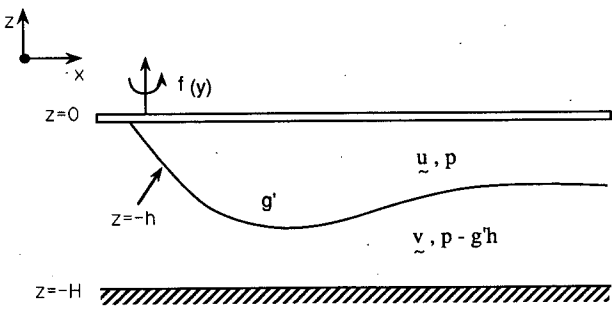

FIG. 1. Model schematic. Upper-layer velocities are denoted by $\mathbf{u}$ and lower-layer velocities by $\mathbf{v}$. The bottom is assumed to be flat (total depth H) and the upper layer is of scale depth H_1. The Coriolis parameter, f, varies with north–south position y.

We have in mind modeling the inertial recirculation, a subject of considerable recent theoretical study. A common theme of the relevant, modern literature is that the recirculation is related only indirectly to wind forcing. This is implicit, for example, in the studies of Marshall and Nurser (1986) and Cessi et al. (1987, CIY hereafter). The thrust of CIY is that the recirculation is forced by anomalous potential vorticities around the edges of the basins. These result from, say, northward advection of low potential vorticity water in a highly inertial western boundary current. Aside from these inhomogeneous boundary conditions, the model is unforced. Marshall and Nurser (1986) also demonstrate the utility of free modes in modeling the inertial recirculation, suggesting that the requisite functional relationship of potential vorticity and streamfunction reflects model driving and dissipation.

In keeping with these studies, the explicit inclusion of wind forcing will be neglected in the present model. Following Marshall and Marshall (1992), fluid will be set in motion by inflow conditions on the western boundary (see Fig. 2). We will impose these in the center of the western boundary and will for simplicity center our coordinate system ($x = y = 0$) on the inflow axis. We will make no effort to resolve the western boundary-layer dynamics, which ultimately set the potential vorticity profile at the inlet; rather, we will assume they are known. This is, of course, a weakness of the model but is typical of large-scale circulation studies.

It is also accepted that the scales of the recirculation are distinguished from those of the general circulation by being "smaller." We will be more quantitative about the scales involved in the next subsections, but we mention here that our strategy will be to consider the inertial recirculation as a "boundary zone" of smaller scale within a large-scale basin. This scale distinction will be of fundamental importance in setting the dynamics appropriate to each zone.

a. Planetary-scale flows

The basin is assumed to be of planetary scale, $L_\beta = (f_0/\beta)$; it is well known that the baroclinic structure of such a fluid is governed by some variant of the planetary geostrophic thermocline equation [for a more complete analysis of the PGTE, see Dewar (1987)]. The barotropic component of the flow obeys a Sverdrup constraint which here, in view of the lack of any wind forcing, identically vanishes. Accordingly, the PGTE ultimately yields the result

$$\beta(H - h)h_x = 0. \tag{2}$$

The solution of (2) is simply that the thermocline is everywhere flat and at a depth determined by the uniform eastern boundary thickness value. It is clear then that the flow in both layers vanishes. This result may seem trivial, but is discussed here in order to emphasize the role of β in setting this structure. The appearance of β reflects the planetary wave dynamics responsible for propagating the eastern boundary influence into the interior, implying that the interior thermocline is dynamically maintained at the depth of the eastern boundary value.

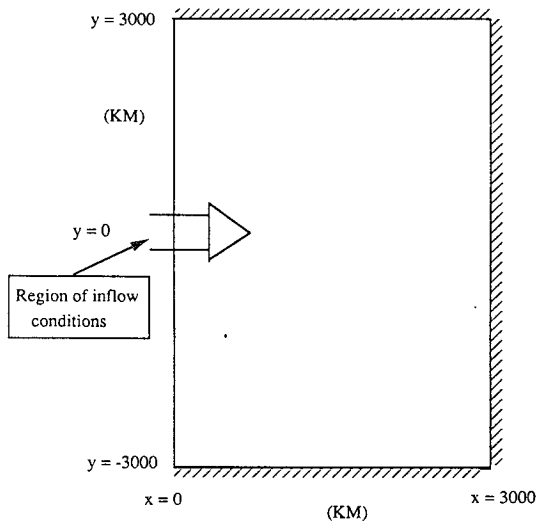

FIG. 2. Basin schematic. Interior motion is forced by inflow boundary conditions on the western boundary. The inflow axis occurs at $y = 0$ and the western boundary is denoted $x = 0$.

This stagnant solution, required by the large-scale dynamics, in general, will be inconsistent with the previously mentioned smaller-scale inflow conditions prescribed on the western boundary, and must somehow be modified to accommodate them. In what follows, we assume the response to those conditions is local, rather than global, and look for a smaller-scale response to the inflow.

b. Recirculation scales

We now develop the equations that govern the recirculation. A reviewer has rightly pointed out a correspondence between a limiting case of our final equations and a particular limiting case of quasigeostrophic dynamics. The quasigeostrophic limit is, of course, of conceptual value because it is simpler, and thus we have included it in an Appendix. We proceed here with our nonquasigeostrophic (and more tedious) analysis because 1) our particular parameter choices are motivated by data and it is of interest to follow the theoretical consequences of observations, and 2) quasigeostrophic dynamics neglects the nonlinearity resident in the continuity equation, which ultimately turns out to be at the heart of our model of internal fronts.

In the inertial recirculation it is observed that isopycnal depth variations, δh, can be comparable to the average depth of the isopycnal. Therefore, this measure of nonlinearity, $\delta h/H_1$ (where H_1 is a scale depth of

the upper layer), will be accepted as O(1) at the outset, which implies that pressure scales as $g'H_1$. Given then that one expects the flow to be approximately geostrophic, upper-layer velocity should scale as $U \sim f_0 R_d^2/L$, where L is the length scale of the flow and $R_d^2 = g'H_1/(f_0^2)$ is the square of the usual deformation scale. The inertial recirculation is also recognized as an area where the flow has an important barotropic component. Certainly, this is the conclusion of Cessi (1988, 1990), Cessi et al. (1987), and Marshall and Nurser (1988), who have examined the recirculation in quasigeostrophic and primitive equation models, and of Schmitz (1980), who has examined North Atlantic current meter data. Therefore, the above scale for $\mathbf{u}$ will also be adopted for $\mathbf{v}$.

Since the system is not driven, and the flow in the inertial boundary zone must still cross lines of constant latitude, relative vorticity must be as important as planetary vorticity in the overall vorticity dynamics. The ratio describing the relative order of these effects is

$$\frac{\beta v}{u v_{xx}} \sim \frac{\beta L^3}{f_0 R_d^2},$$

which when set to O(1) selects the parameter "L" to be the intermediate scale

$$L = L_I = (R_d^2 L_\beta)^{1/3}, \tag{3}$$

where $L_\beta = f_0/\beta$ is the planetary scale (Charney and Flierl 1981). Note, $L_I \ll L_\beta$, consistent with our boundary-layer approach to this problem. Typical parameters ($R_d \sim 40$ km, $L_\beta \sim 3000$ km) yield $L_I \approx 200$ km. For comparison, Schmitz (1980) finds from current meter data that the westward-flowing zone of the inertial recirculation has a 200-km meridional scale, suggesting an oceanographic relevance for L_I. This will be used as the fundamental length scale in what follows.

The nondimensional forms of (1) appropriate to the region of the inflow boundary conditions are thus

$$\epsilon^2(\mathbf{u}\cdot\nabla\mathbf{u}) + (1+\epsilon^2 y)\mathbf{k}\times\mathbf{u} = -\nabla p_1 = -\nabla(p+h) \tag{4a}$$

$$\nabla\cdot(\mathbf{u}h) = 0 \tag{4b}$$

$$\epsilon^2(\mathbf{v}\cdot\nabla\mathbf{v}) + (1+\epsilon^2 y)\mathbf{k}\times\mathbf{v} = -\nabla(p) \tag{4c}$$

$$\nabla\cdot[\mathbf{v}(1-\hat{\delta}h)] = 0, \tag{4d}$$

where $\epsilon^2 = (R_d/L_I)^2 \equiv (L_I/L_\beta)$ and $\hat{\delta} = H_1/H$ appear as the two parameters of the system. Further, "p" appearing in (4a) and (4c) denotes the nondimensional form of *lower*-layer pressure. Typical oceanic values lead to $\epsilon^2 \sim 0.06$, while $\hat{\delta} = (500\text{–}1000)$ m/500 m $\sim (0.1 \sim 0.2)$. Note that $\hat{\delta}$ lies in the range of ϵ to ϵ^2. We will adopt the scaling $\hat{\delta} \sim \epsilon$ here and state immediately that the final governing equations turn out to be insensitive to this choice. We define $\hat{\delta} = \epsilon\delta$, where $\delta \sim O(1)$, to simplify our notation.

3. The recirculation and fronts

a. *Solutions for the recirculation*

We now consider an expansion of (4) in ϵ. Clearly, the flow in both layers is geostrophic at O(1) and O(ϵ). A useful constraint is obtained from the O(1) upper-layer continuity equation; that is,

$$J(p_0, h_0) = 0, \tag{5}$$

where J denotes the usual Jacobian operator and subscripts denote the order of the expansion. Equation (5) may be understood by considering potential vorticity conservation. Equations (1a,b) are equivalent to

$$\mathbf{u}\cdot\nabla\left(\frac{h}{\nabla\times\mathbf{u}+f}\right) = 0, \tag{6}$$

where the quantity $(\nabla\times\mathbf{u}+f)/h = q$ is recognized as potential vorticity. Scaling (6) as described above, and expanding, yields:

$$(\mathbf{u}_0 + \epsilon\mathbf{u}_1 + \cdots)\cdot\nabla \times\{h_0 + \epsilon h_1 + \epsilon^2[h_2 - h_0(y + \nabla\times\mathbf{u}_0)] + \cdots\} = 0.$$

Clearly, (5) is the lowest-order constituent of the above. Heuristically, at the L_I scale, both β and relative vorticity are weak in strength. Column thickness, h, on the other hand is subject to large variations. The upper-layer flow, being approximately geostrophic, therefore satisfies potential vorticity conservation by adhering to Taylor–Proudman flow.

The O(1) form of lower-layer continuity is simply $\nabla\cdot\mathbf{v}_0 = 0$, which is automatically satisfied by geostrophy. At O(ϵ), lower-layer continuity yields $\nabla\cdot\mathbf{v}_1 - \delta\nabla\cdot\mathbf{v}_0 h_0 = 0$, which in view of (5) reduces to simple nondivergence of $\mathbf{v}_1$. The O(ϵ) lower-layer dynamics are seen to be identical to the O(1) dynamics and introduce nothing new. Thus, with no loss of generality, $\mathbf{v}_1$ and hence the correction to p_2 may both be set to zero. The O(ϵ) upper-layer momentum equations consist of simple geostrophy, and the use of earlier results in O(ϵ) continuity yields $J(p_0, h_1) = 0$. Manipulation of this result and (5) demonstrates h_1 and h_0 are functionally related, so h_1 may be set to zero, again with no loss of generality. Hence, $\mathbf{u}_1 = 0$ and all O(ϵ) corrections are seen to vanish. To acquire a second constraint to complement (5), and close the problem in the recirculation zone, requires expansion to O(ϵ^2). This is not surprising as at this order resides relative vorticity and beta.

It is necessary to consider only the lower-layer equations at O(ϵ^2), which in view of the O(ϵ) results yield nondivergence of $\mathbf{v}_2$, and a second constraint on p_0; namely,

$$J(p_0, \nabla^2(p_0) + y) = 0. \tag{7}$$

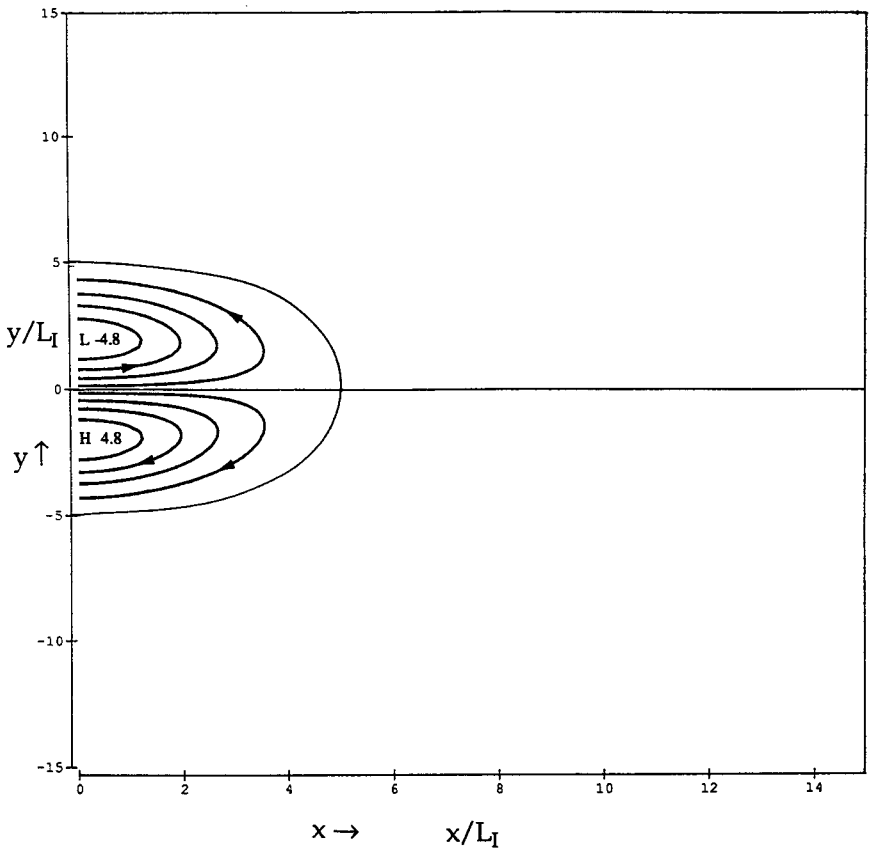

FIG. 3. Lower-layer pressure p (nondimensional). The critical radius a is chosen to be 1000 km ($a = 5$) and the basin is assumed to be 6000 km × 3000 km. Maximum speeds are O(10 cm s^{-1}).

The above is immediately recognized as the steady form of the absolute vorticity equation on a beta plane. The scaling for $\hat{\delta}$ in combination with the baroclinic result (5) is sufficient to ensure that vortex tube stretching is a weak effect on the flow. Equations (5) and (7) form a closed set for p_0 and h_0 in the inertial boundary zone.

Note that (7) is one equation in the one unknown p_0, representing lower-layer pressure, and can be solved subject to an absolute vorticity specification for the jet (which will be applied at the inlet). Note that because we do not explicitly model the western boundary layer, we are unconcerned with the outflow conditions. The content of (5) and (7) is that once p_0 is obtained, h_0 can be calculated from a specification of h_0 on pressure lines at the inlet.

We will assume here for analytical convenience a linear functional form between absolute vorticity and streamfunction. Thus, the lower-layer inertial recirculation structure will be governed by

$$\nabla^2(p_0) + y = -B^2(p_0), \tag{8}$$

whose solution is

$$p_0 = DJ_1(Br)\sin\theta - y/B^2, \tag{9}$$

where J_1 denotes the Bessel function of the first kind of order 1 and D is an as yet unknown constant. The quantities r and θ are the coordinates of a cylindrical system centered on the jet axis at $x = y = 0$. [The remaining solutions of (8) proportional to higher-order trigonometric functions of θ are neglected in anticipation of the boundary conditions.] The far field conditions on p_0 are set by (2) and require that both pressure and velocity vanish. The simplest way to meet these constraints is by choosing a critical radius $r = a$ where they are applied. For simplicity here, we will always choose $a < x_e$, where x_e is the location of the eastern boundary. This is also consistent with the scaling $L \sim L_I \ll L_\beta$. The resulting solution for lower-layer pressure is thus

$$p_0 = \frac{a}{B^2 J_1(Ba)} J_1(Br)\sin\theta - y/B^2, \tag{10}$$

where B and a are further related by the requirement $J_2(Ba) = 0$[J_2 being the Bessel function of order 2]. Equation (10) should be recognized as the eastern half of the Stern (1975) barotropic modon. Here, this flow pattern will be referred to as the inertial recirculation. The solution appropriate to (10) is shown in Fig. 3.

At least two points (or perhaps apologies) should be made about this solution. The first is that it is necessary that the coefficient of the streamfunction in (8), here written as $-B^2$, be negative to obtain such a solution. This can be demonstrated by noting that such an absolute vorticity function cannot produce a westward flow in which relative vorticity is negligible. On the positive side, a consequence of assuming a coefficient like $-B^2$ is that the inflow jet profile has a "smooth" form as sketched in Fig. 4a as opposed to the "cusplike" profile sketched in Fig. 4b. The former profile is associated with an absolute vorticity that is smooth; the cusplike current profile in Fig. 4b implies a discontinuity in the absolute vorticity profile at the current axis. A smooth absolute vorticity profile in the deep layers is perhaps to be preferred on the physical grounds that no deep potential vorticity sources exist that can maintain a mean absolute vorticity front. The second point is that this solution is clearly very special, and coincides with a heavily constrained profile at the inlet. Varying the inflow profile can be expected to alter the details of the recirculation. With regard to this last point, Marshall and Marshall (1992; MM hereafter) have studied the penetration versus recirculation properties of a seaward-flowing jet and shown how it is controlled by its cross-stream velocity profile. In a barotropic model they demonstrated that if the streamfunction coefficient of the inflowing jet is negative (as here), corresponding to a smooth inflow profile, a recirculating Stern modon is resonantly excited; conversely, if the coefficient is positive, a penetrating Fofonoff mode is excited. In multilayer models it is the coefficient associated with the barotropic mode (or strictly speaking the pseudobarotropic mode) that is the controlling parameter.

A notable result of MM is that subtle changes in the jet profile, with relatively small admixtures of a Stern-like inflow profile to an otherwise Fofonoff-like jet, lead to interior *recirculation.* For example, Fig. 5 taken from MM shows steady flow patterns obtained by injecting fluid into a half-basin in a series of numerical experiments in which an inflow profile is incrementally changed from a Fofonoff inflow (with a cusplike profile) to an increasingly modonlike inflow (with a smooth profile). We see that as the profile becomes smoother, rather than penetrating across to the eastern boundary, the inflow jet adjusts to the presence of a no-flux condition by recirculating and creating a free streamline in the interior region.

In the present study, the barotropic mode is dominated by the lower-layer flow because the lower layer is deep. Thus, our choice of a negative coefficient, implying recirculating behavior and a smooth cross-stream vorticity profile, is entirely consistent with the study of MM.

Last, many of the recent inertial recirculation studies have assumed uniform potential vorticity in the recirculation zone, this being viewed as the end state pro-

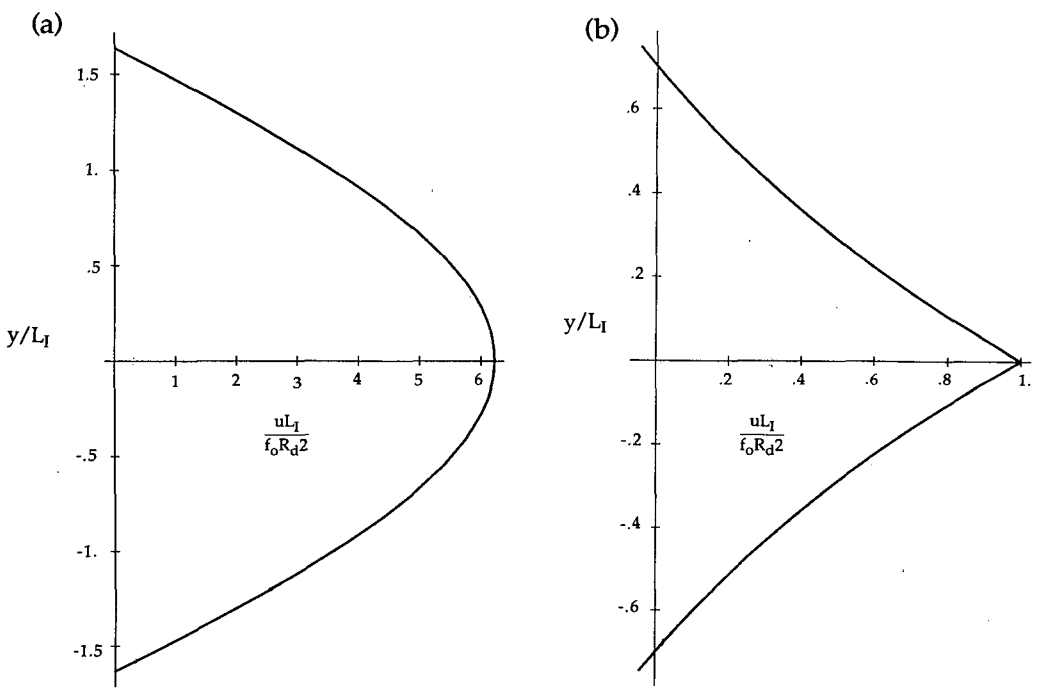

FIG. 4. Lower-layer inflow profiles. Potential vorticity is assumed to be a linear function of pressure. In (a) the linear coefficient is negative, while in (b) the coefficient is positive. The profile in (b) maintains a potential vorticity front along the inflow axis, while the potential vorticity is smooth in (a). The profile in (a) is used in the present calculations.

duced by eddy mixing (e.g., see Cessi 1990). In contrast, the functional relationship we adopt in (8) is not uniform; rather it is a linear function of a streamline. Nonetheless, note we are not working with potential vorticity here; rather, we are working with absolute vorticity, as required by the analysis. Further, adjusting our functional relationship by including thermocline topography moves it in the direction of uniform potential vorticity. To see this, note that dimensional lower-layer potential vorticity in our model is given approximately by

$$q = \nabla \times \mathbf{v} + f_0 + \beta y + \frac{f_0 h}{H},$$

where the thickness of the lower layer has been explicitly recognized. In view of (8), the above can be rewritten

$$q = -\mu^2 p_0 + \frac{f_0 h}{H} + f_0,$$

where $\mu^2 = B^2/f_0 L^2$ is the dimensional version of B^2 in (8). Clearly from (5) thickness and lower-layer pressure are related. One further expects their correlation to be positive as greater (lesser) thicknesses occur in the anticyclonic (cyclonic) subtropical (subpolar) gyre. Thus, the thickness contribution to potential vorticity opposes the absolute vorticity component in sign and, indeed, a judicious choice for h can result in uniform q. Thus, our analysis here does not in principle represent a departure from previous uniform potential vorticity ideas. To summarize, then, we adopt the Stern modon as a convenient analytical example of a free inertial recirculation.

The solution of (5) is

$$h_0 = F(p_0), \tag{11}$$

which, given (10), can easily be determined by the conditions on h_0 at the jet inlet. Contours of constant depth then simply overlie contours of constant lower-layer pressure. The obvious constraints to place on F are that it should have a maximum in the subtropical gyre and a minimum in the subpolar gyre. An example with h_0 linearly proportional to p_0, and varying between a maximum of 800 m and outcropping, is shown in Fig. 6. A particularly important quantity is the upper-layer thickness on the jet axis, here denoted by h_{0c}. Note that (11) requires $h_0 = h_{0c}$ on the bounding free streamline at $r = a$.

Given that the separation radius a lies within the basin, the thermocline outside of the inertial recirculation is set by other processes, here given by (2). This determines h_0 in the far field to be the eastern boundary thickness, h_e, due to the presence of β.

If $h_e = h_{0c}$, the thermocline is smooth and continuous, and the first-order structure of the basin is complete. On the other hand, if $h_e \neq h_{0c}$, then the solution thus far predicts a discontinuity in h at the boundary of the recirculation. This, of course, requires a singularity in the velocity field and is an indication that the analysis must proceed further. We now examine this case.

b. Internal fronts

First, note that the inconsistency in the solution (i.e., the singularity) involves h_0 and not p_0. Also, in some sense, it is seen that the discontinuity is a consequence of the simple first-order nature of the equations determining h_0. Equations (2) and (11) by themselves have characteristics that intersect at the edge of the recirculation, suggesting that in the vicinity of the intersection, another smaller scale emerges and dynamics that were locally unimportant previously become of first-order importance. Clearly, then, the scaled equations (4) must lose validity in the vicinity of $r = a$.

If (1a–d) are again nondimensionalized, but with the length scale of the flow, L, left as a free parameter, we obtain

$$\left(\frac{R_d}{L}\right)^2 (\mathbf{u}\cdot\nabla\mathbf{u}) + \left(1 + \frac{L}{L_\beta} y\right)\mathbf{k}\times\mathbf{u} = -\nabla p(p + h), \tag{12a}$$

$$\nabla\cdot(\mathbf{u}h) = 0, \tag{12b}$$

$$\left(\frac{R_d}{L}\right)^2 (\mathbf{v}\cdot\nabla\mathbf{v}) + \left(1 + \frac{L}{L_\beta} y\right)\mathbf{k}\times\mathbf{v} = -\nabla(p), \tag{12c}$$

$$\nabla\cdot[\mathbf{v}(1 - \hat{\delta}h)] = 0, \tag{12d}$$

from which it is seen that the dynamics that become more important as L decreases are the inertial terms and, furthermore, may become order one for $L \approx R_d$. Equating L and R_d, (12) yields the steady-state f-plane equations at lowest order. Recall that these apply in the vicinity of the inertial recirculation boundary, $r = a$.

Since the f-plane equations have no preferred orientation, they can be written in cylindrical coordinates, which near $r = a$ are in effect a system locally oriented along and across the inertial recirculation boundary. It is furthermore appropriate to look for anisotropic solutions to these equations, since the alongfront scale is set by the recirculation and is $O(L_1) \gg R_d$. Scaling arguments then show that the equations appropriate to the edge of the inertial recirculation are the semigeostrophic equations; that is:

$$u^\theta = (p + h)_r \tag{13a}$$

$$u^r u^\theta_r + \frac{u^\theta}{a} u^\theta_\theta + u^r = -\frac{1}{a}(p + h)_\theta \tag{13b}$$

$$(u^r h)_r + \frac{1}{a}(u^\theta h)_\theta = 0 \tag{13c}$$

$$v^\theta = (p)_r \tag{13d}$$

$$v^r v^\theta_r + \frac{v^\theta}{a} v^\theta_\theta + v^r = -\frac{1}{a}(p)_\theta \tag{13e}$$

$$(v^r)_r + \frac{1}{a}(v^\theta)_\theta = 0, \tag{13f}$$

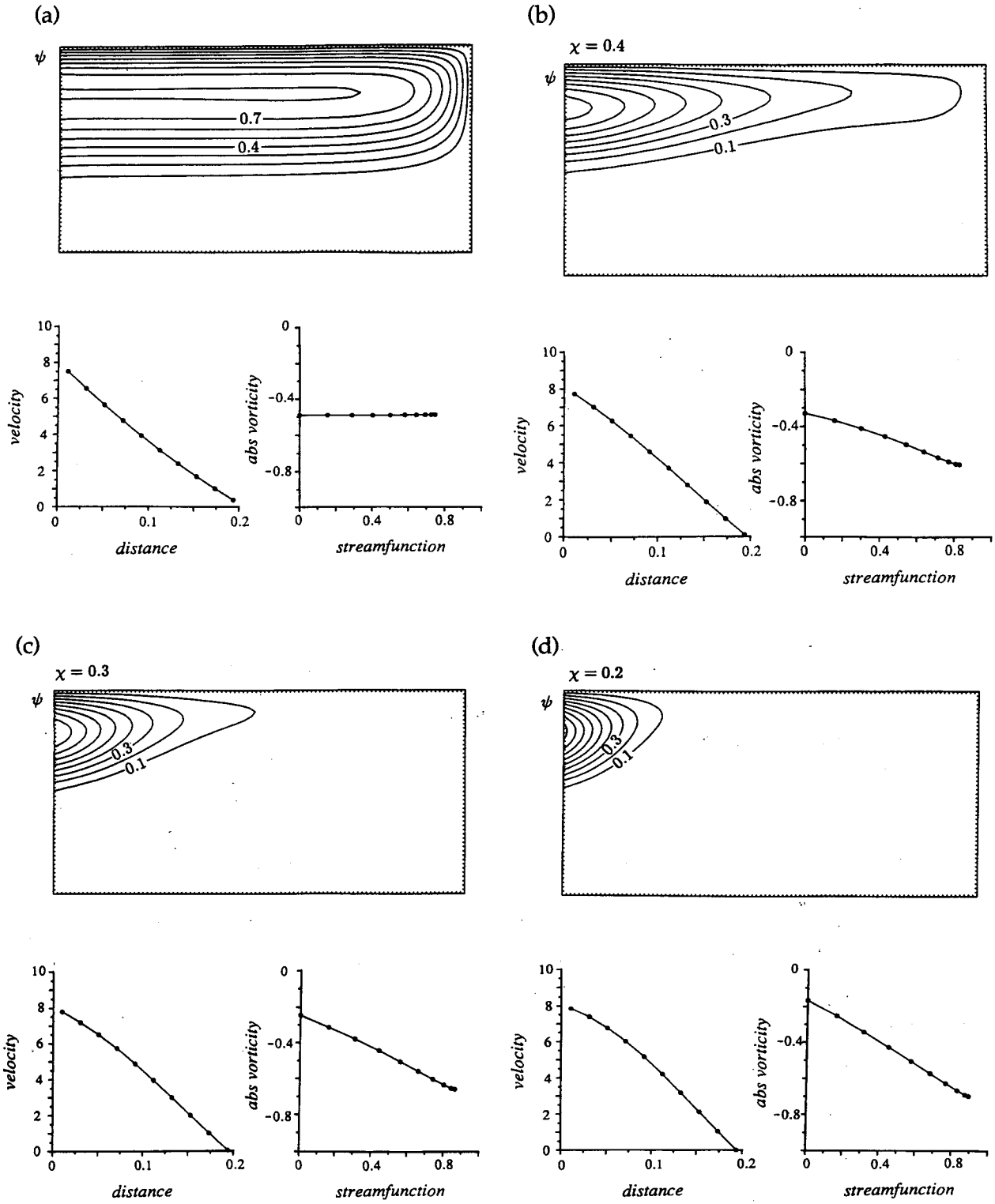

FIG. 5. A sequence of steady states obtained from numerical integration of the barotropic vorticity equation in a half-basin. Details of the model can be found in Marshall and Marshall (1992). An inflow in the northwest corner of the subtropical gyre is prescribed as a "mix" of modon and Fofonoff type solutions; the outflow to the west is allowed through radiation boundary conditions. The quantity χ denotes the fraction of Fofonoff type inflow at the port. In (a) $\chi = 1$; (b) $\chi = .4$; (c) $\chi = .3$; (d) $\chi = .2$. The two graphs in each panel show the jet profile at the inflow and the functional relationship between absolute vorticity and streamfunction (B^2) at the inflow port. There is a striking sensitivity of the penetration scale of the jet to the form of the inflow profile. If the cross-stream velocity profile is cusplike, the jet penetrates

where the quantities $u^r(v_r)$ and $u^\theta(v_\theta)$ are the upper (lower) layer, lowest-order radial and azimuthal components of velocity, that is, $(u^r, u^\theta) = \mathbf{u}$, and $(v^r, v^\theta) = \mathbf{v}$, and subscripts denoting order have been suppressed. The quantity r is the cross-front coordinate and θ is the alongfront coordinate. It is also true that (13) conserve potential vorticity in the form

$$\mathbf{u}\cdot\nabla\left(\frac{u_r^\theta + 1}{h}\right) = 0 \qquad (14a)$$

for the upper layer and

$$\mathbf{v}\cdot\nabla(v_r^\theta) = 0 \qquad (14b)$$

for the lower layer.

In view of the semigeostrophic approximation, (14b) yields

$$(p)_{rr} = F(\psi_2), \qquad (15)$$

where F denotes the potential vorticity functional and ψ_2 the lower-layer mass transport streamfunction. Clearly, the solution of (15) depends upon F, which is ultimately given by boundary conditions. In view of the fact that both the velocity and pressure of the lower-layer inertial recirculation solution in (10) match smoothly to the large-scale solution at $r = a$, we will adopt here the solution for which the lower layer is stagnant in this deformation scale internal boundary layer, which implies

$$p = 0. \qquad (16)$$

This, in effect, says the lower-layer has no internal boundary-layer structure imposed on it.

In view of (16), (14a) yields

$$h_{rr} + 1 = hG(\psi_1), \qquad (17)$$

where ψ_1 is the upper-layer mass transport streamfunction. A second constraint relating h_0 and ψ_1 may be obtained from a Bernoulli principle.

The boundary conditions on (17) are that $h \to h_e$ as $r \to \infty$, and $h \to h_{0c}$ as $r \to -\infty$. The fact that $h_{0c} \neq h_e$ requires the presence of the deformation-scale boundary layer, unlike the situation in the lower layer. The boundary layer serves to smoothly join the far field in both thickness and velocity as shown in Fig. 7.

The potential vorticity structure function G is, in principle, set on the west (see Fig. 6), and the details of the front and the associated jet structure depend somewhat upon it. An example is shown in Fig. 7 where the potential vorticity of the jet consists of the two uniform values $1/h_{0c}$ to the west and $1/h_e$ to the east.

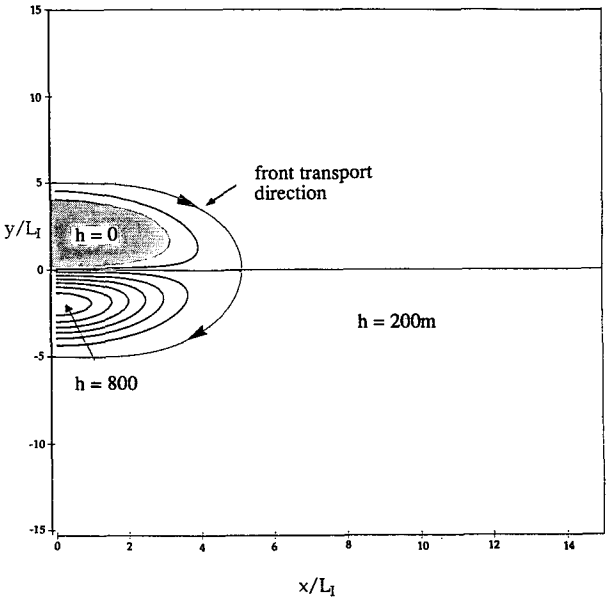

FIG. 6. Thermocline structure. The lower-layer pressure pattern is given in Fig. 3. The thermocline in the recirculation goes from a maximum depth of 800 m in the subtropical gyre to an outcrop in the subpolar gyre. The arrow indicates the flow direction of the internal boundary layer on the rim of the circulation. The southward direction is consistent with a shallower thermocline east of the front.

On the other hand, the net jet transport is insensitive to the potential vorticity structure and depends only upon the far-field conditions:

$$\int_{-\infty}^{\infty} (hu^\theta)dr = \frac{h_e^2}{2} - \frac{h_{0c}^2}{2}. \qquad (18)$$

With the addition of the internal boundary layer, the upper-layer thickness, pressure, and velocity fields are rendered smooth and continuous, and the lowest-order description of the interior is complete.

c. *Application to the LDE jet*

The model presented above is highly idealized, but we are nonetheless interested in assessing if it has anything of use to say about real ocean jet dynamics. We therefore attempt here an application of the model to the LDE jet. To do so entails a number of questionable assumptions; for example, the model is steady while the LDE jet was observed to move through the LDE array at a speed of $\sim$4 cm s^{-1}. Further, we are working with a two-layer representation of a continuously stratified ocean and ignoring explicit wind-driven circula-

FIG. 5. (*Continued*). effectively across the basin; if it is smooth, the flow recirculates. Distance is nondimensionalized with respect to L, the meridional extent of the basin. The streamfunction is presented in units of $10^{-2}\beta L^3$, where β is the planetary vorticity gradient, absolute vorticity is in units of βL, and the velocity is in units of $10^{-2}\beta L^2$. Thus if $\beta = 1.6 \times 10^{-11}$ s^{-1} m^{-1} and $L = 500$ km, then a nondimensional velocity of unity corresponds to a current speed of 4 cm s^{-1}; thus, the jet peaks at a speed of 30 cm s^{-1}.

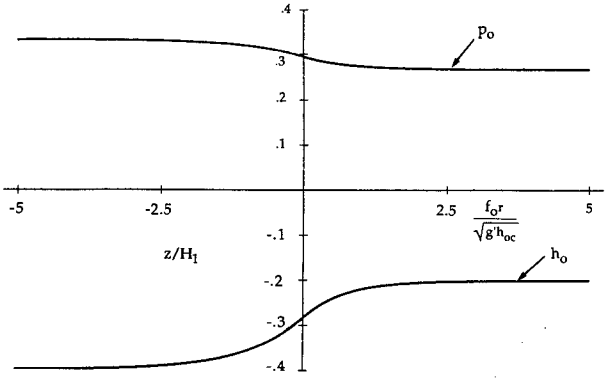

FIG. 7. Pressure and thickness transition in the jet. The jet constitutes an internal deformation scale boundary layer that smoothly joins the far field thermocline values. Because the front occurs on the inertial recirculation boundary, $p \approx h$ and the lower-layer flow is stagnant to leading order. The magnitude of the p variation appears smaller than that of h because of a scaling and is meant to reflect that p is associated with free surface variations.

tion. However, in spite of the idealized nature of our study, there are some comparisons with the observed LDE jet characteristics that are worthwhile.

The observed parameters of the LDE jet, obtained during the Intensive Hydrographic Program, were that it had a finite isopycnal depth change across the front of approximately 200 m, consisting of a shallowing of the isopycnals moving east across the front and the strongest jet velocities were observed near the surface. It was also observed that the flow at depths of up to 3000 db was in the same direction as the surface flow, suggesting that the jet may have been a full column event. The net transport of the jet relative to 3000 db was estimated at 40 Sv. This latter interpretation of jet vertical structure, however, is complicated by two points. First, it has been argued that the deep velocities at the time of the jet belong to a topographic planetary wave (Price and Rossby 1982), which suggests that their appearance at the LDE site at the time of the jet was only fortuitous. Second, a jetlike feature was observed at the LDE site in May 1979, one year after the event formally referred to as the LDE jet. This second jet did not possess the high degree of vertical coherence of the LDE jet. Thus, the vertical structure of the LDE jet is not terribly clear, apart from the idea that its strongest velocities occurred at the surface. We shall therefore focus on this latter feature in what follows. A crude estimate suggests that 50%–60% of the estimated 40-Sv jet transport lies in upper kilometer of the fluid column.

To apply the present model to the LDE jet requires that h_{0c} be identified with the western jet thickness and h_e with the eastern thickness, which is assumed to be shallower. No explanation is provided by the present analysis as to why the inertial recirculation thickness should differ from the eastern thickness; rather, it is simply noted that the model permits such boundary conditions. (We do speculate, however, that the processes controlling the eastern boundary stratification are likely to be very different from those controlling the west, and thus that there is no obvious a priori reason that the two should be identical. Further, the fact that subtropical circulations are warmer in the west may well predispose them toward internal fronts that, like the LDE jet, are thicker on the west.)

Having made this identification, it should be noted that the surface intensification of the jet, the order of magnitude of the transport anomaly, and the direction of the transport anomaly are accounted for by the present model. In particular, dimensionalizing (18) and using $g' = 1.5$ cm s^{-2}, $h_{c0} = 10^5$ cm, $h_e = 8.0 \times 10^4$ cm, and $f = 10^{-4}$ s^{-1} yields

$$T = \int_{-\infty}^{\infty} hu^{\theta} dr = \frac{g'}{2f_0}[h_e^2 - h_{c0}^2] \cong -27 \text{ Sv},$$

where the minus sign indicates the southward orientation of the mass flux.

Note that (18) is independent of latitude, demonstrating that the origin of the mass flux is in the subpolar basin, in particular, on the subpolar western boundary. (Recall that the h_e, h_{0c} differential is maintained everywhere on the $r = a$ boundary, including the subpolar gyre and at the separating latitude of the subtropical and subpolar gyres.) The validity of the present model thus presupposes that the western boundaries are capable of generating such a mass flux. Assumptions like this are typical of several modern circulation theories (e.g., Rhines and Young 1982; Luyten et al. 1983; Schopp and Arhan 1986), but they still represent a weakness of the present analysis. It is nonetheless interesting to reconsider the pathways of some of the water mass anomalies observed during the LDE in light of our results.

Using the finescale, deep, and repeated nature of the hydrographic part of the LDE, individual water parcels of anomalous heat and salt content (relative to the background) were detected and tracked. These data were combined with historical observations to determine potential source regions for the anomalies, as well as to arrive at estimates for the numbers of such anomalies in the North Atlantic. Details of the procedure can be found in Ebbesmeyer et al. (1986). Elliott and Sanford (1986a,b) focus on one particular subthermocline anticyclone, which they named D1. This anomaly was distinguished by low salinities ultimately traceable to the Labrador Sea. Elliott and Sanford argue that the formation zone of D1 was located near the southeast corner of the Grand Banks, a place to which nearly pure Labrador Sea water is advected by western boundary currents. They also speculate that D1 moved east after formation in an interaction with the Gulf Stream, was entrained into the recirculation, and eventually carried to the LDE site.

We mention here that at its proposed formation longitudes (50°–55°W), D1 was actually north of the

Gulf Stream, possibly by some few hundreds of kilometers. It is interesting to note that this location roughly corresponds to the jet origin location in our model. Further, the history of D1 within the LDE area was reported on by Lindstrom and Taft (1986). Comparing the sequence of locations where D1 was observed with the 1300-db streamfunction maps of Hua et al. (1986) shows that D1 was embedded in, and being advected by, the LDE jet. It seems then that the present study can provide a mechanism for the observation of D1 at the LDE experimental site, as well as the existence of the LDE jet (in which D1 was found). From the viewpoint of the anomaly, the present model jet constitutes a dynamically consistent pathway across the Gulf Stream, from a generation spot on the subpolar western boundary, to the LDE site.

4. Summary

A simple inertial model of embedded jets has been developed. The substance of the model is that a potential vorticity conserving current, flowing eastward from an inlet zone, can satisfy a no-flux condition on the east by forming a free streamline and recirculating in the interior. The scale of the recirculation is the intermediate length, $L_I \approx 200$ km, which compares favorably with the observed scale of the North Atlantic recirculation. In a system with a deep but active lower layer, the baroclinic response is almost passive—that is, thickness contours follow pressure contours. The fluid outside the recirculation is governed by large-scale dynamics; thus the eastern boundary sets the far-field baroclinic structure by dynamics in which β plays a pivotal role.

If these two separate processes result in different upper-layer thicknesses at their common boundary, a deformation scale internal boundary layer is formed that smoothly joins the two regions. Thus the existence of a baroclinic front reflects the presence of inconsistent boundary conditions on the east and the west. The jet associated with the boundary layer has a source on the subpolar western boundary (if $h_{0c} > h_e$), and is surface intensified. Applying this model to the LDE data yields some suggestive comparisons. In particular, the order of magnitude of the observed jet transport, the direction of the jet flow and the presence of anomalous water masses within the jet have an interpretation with the model.

One major shortcoming of this model lies in the neglect of western boundary layer dynamics. Their effect is parameterized by means of the potential vorticity–streamfunction relationship for the inflow, and it is assumed that the western boundary, away from the Gulf Stream axis, can supply the mass required by the interior jet. The latter is the strongest model prediction (or perhaps constraint) regarding the interior jet and points out clearly a question of considerable observational interest. It immediately becomes of central importance to determine the source region of the anomalous LDE jet transport. From an observational point of view, one must admit the possibility that the Gulf Stream itself might have fed the requisite mass to the LDE jet. This is inconsistent with our theory. If so, the LDE jet dynamics are not adequately addressed by the present model, and must await future clarification. The scenario in the present model points to source zones in the subpolar gyre and a subsequent intergyre mass exchange to supply the LDE jet with mass. Determining which of these mechanisms applies (or if an entirely different mechanism is required to account for the LDE transport source) remains a question that future relevant observational programs might wish to consider.

Acknowledgments. WKD would like to acknowledge ONR Contract N00014-89-J-1577 and NSF Grant OCE 902114 for support of this work. JCM would like to acknowledge NSF Grant OCE 9115915. Ms. Sheila Heseltine is thanked for preparing the manuscript and Mr. J. Park assisted in the production of the figures. This work was begun during a discussion by the authors at the 1991 WHOI GFD Summer School.

APPENDIX

A Quasigeostrophic Expression of Inertial Recirculation

We begin with the dimensional two-layer quasigeostrophic equations; namely,

$$J(\psi_1, \nabla^2\psi_1 + \beta y + f_0^2\psi_2/g'H_1) = 0, \quad \text{(A1)}$$

$$J(\psi_2, \nabla^2\psi_2 + \beta y + f_0^2\psi_1/g'H_2) = 0, \quad \text{(A2)}$$

where $\psi_1 = p_1/f_0$ and $\psi_2 = p_2/f_0$ are the upper- and lower-layer streamfunctions. The quantities p_1 and p_2 are upper- and lower-layer dynamic pressure and other notation is standard.

These equations can be manipulated into the forms

$$J(\psi_1, \psi_2) = -\frac{g'H_1}{f_0^2} J(\psi_1, \nabla^2\psi_1 + \beta y), \quad \text{(A3)}$$

$$J(\psi_2, \nabla^2\psi_2 + \beta y) = \frac{H_1}{H_2} J(\psi_1, \nabla^2\psi_1 + \beta y), \quad \text{(A4)}$$

whose left-hand sides are clearly the *qg* analogs of (5) and (7). The conditions under which the right-hand sides are of negligible importance are seen to be $U \sim \beta L^2$, $L^2 \gg g'H_1/f_0^2$ and $H_1 \ll H_2$. Thus, an analog to our system is found in this asymptotic limit of *qg* dynamics, which emphasizes the importance of inertia and large scales. To examine the possibility of a sizeable baroclinic front, however, requires a more complete consideration of the nonlinearity in the continuity equation.

REFERENCES

Cessi, P., 1988: A stratified model of the inertial recirculation. *J. Phys. Oceanogr.*, **18**, 662–682.

——, 1990: Recirculation and separation of boundary currents. *J. Mar. Res.*, **48,** 1–35.

——, G. Ierley, and W. Young, 1987: A model of the inertial recirculation driven by potential vorticity anomalies. *J. Phys. Oceanogr.*, **17,** 1640–1652.

Charney, J. C., and G. R. Flierl, 1981: Oceanic analogues of large scale atmospheric motions. *Evolution of Physical Oceanography,* B. A. Warren and C. Wunsch, Eds., The MIT Press, 504–548.

Cushman-Roisin, B., 1984: On the maintenance of the subtropical front and its associated countercurrent. *J. Phys. Oceanogr.*, **14,** 1179–1190.

Dewar, W. K., 1987: Planetary shock waves. *J. Phys. Oceanogr.*, **17,** 470–482.

——, 1991a: Arrested fronts. *J. Mar. Res.*, **49,** 21–52.

——, 1991b: Spontaneous shocks. *J. Phys. Oceanogr.*, **21,** 505–522.

Ebbesmeyer, C., B. A. Taft, J. C. McWilliams, C. Y. Shen, S. C. Riser, H. T. Rossby, P. E. Biscayne, H. G. Ostlund, 1986: Detection, structure and origin of extreme anomalies in a western Atlantic oceanographic section. *J. Phys. Oceanogr.*, **16,** 591–612.

Elliott, B. A., and T. B. Sanford, 1986a: The subthermocline lens D1. Part I. Description of water properties and velocity profiles. *J. Phys. Oceanogr.*, **16,** 532–548.

——, and ——, 1986b: The subthermocline lens D1. Part II. Kinematics and dynamics. *J. Phys. Oceanogr.*, **16,** 549–561.

Hua, B., J. C. McWilliams, and W. B. Owens, 1986: An objective analysis of the POLYMODE Local Dynamics Experiment. Part II. Streamfunction and potential vorticity fields during the intensive period. *J. Phys. Oceanogr.*, **16,** 506–522.

Lindstrom, E., and B. A. Taft, 1986: Small water property transporting eddies: Statistical outliers in the hydographic data of the POLYMODE Local Dynamics Experiment. *J. Phys. Oceanogr.*, **16,** 613–631.

Luyten, J., and H. Stommel, 1986: Gyres driven by combined wind and buoyancy flux. *J. Phys. Oceanogr.*, **16,** 1551–1560.

——, J. Pedlosky, and H. Stommel, 1983: The ventilated thermocline. *J. Phys. Oceanogr.*, **13,** 292–309.

Marshall, D., and J. Marshall, 1992: Zonal penetration scale of midlatitude jets. *J. Phys. Oceanogr.*, **22,** 1018–1032.

Marshall, J., and G. Nurser, 1986: Steady, free circulation in a stratified quasigeostrophic ocean. *J. Phys. Oceanogr.*, **16,** 1799–1813.

——, and ——, 1988: On the recirculation of the subtropical gyre. *Quart. J. Roy. Meteor. Soc.*, **114,** 1517–1534.

McWilliams, J. C., and Coauthors, 1983: The local dynamics of eddies in the Western North Atlantic. *Eddies in Marine Science,* A. R. Robinson, Ed., Springer-Verlag, 92–113.

Price, J. F., and H. T. Rossby, 1982: Observations of a barotropic planetary wave in the western North Atlantic. *J. Mar. Res.*, **40**(Suppl.), 543–558.

Rhines, P., and W. Young, 1982a: Homogenization of potential vorticity in planetary gyres. *J. Fluid Mech.*, **122,** 347–367.

——, and ——, 1982b: A theory of the wind-driven circulation I. Mid-ocean gyres. *J. Mar. Res.*, **40**(Suppl.), 559–596.

Schmitz, W. J., 1980: Weakly depth-dependent segments of the North Atlantic circulation. *J. Mar. Res.*, **38,** 111–133.

Schopp, R., and M. Arhan, 1986: A ventilated middepth circulation model for the Eastern North Atlantic. *J. Phys. Oceanogr.*, **16,** 344–357.

Stern, M. E., 1975: Minimal properties of planetary eddies. *J. Mar. Res.*, **33**(1), 1–13.